



## Article

# The Effect of a Yb Co-Dopant on the Blue Upconversion and Thermoluminescent Emission of SrLaAlO<sub>4</sub>:Yb<sup>3+</sup>, Tm<sup>3+</sup> Phosphors

Nelson Oshogwue Etafo <sup>1</sup>, Carlos Rodriguez Garcia <sup>1,2</sup>, Tzipatly A. Esquivel-Castro <sup>3</sup>, Manuel I. León-Madrid <sup>4</sup>, Alejandro Santibañez <sup>5</sup> and Jorge Oliva <sup>3,\*</sup>

- <sup>1</sup> Programa de Posgrado en Ciencia y Tecnología de Materiales, Facultad de Ciencias Químicas, Universidad Autónoma de Coahuila, Ing. J. Cárdenas Valdez S/N Republica, Saltillo 25280, Coahuila, Mexico
- <sup>2</sup> Facultad de Ciencias Físico Matemáticas, Universidad Autónoma de Coahuila, Edif. A. S/N, Unidad Camporredondo, Saltillo 25000, Coahuila, Mexico
- <sup>3</sup> CONAHCYT-Instituto Potosino de Investigación Científica y Tecnológica A.C., Camino a la Presa de San José 2055, Lomas 4ta Secc, San Luis 78216, San Luis Potosi, Mexico
- <sup>4</sup> Department of Physical Engineering, DCI, University of Guanajuato, León 37150, Guanajuato, Mexico
- <sup>5</sup> Departamento de Materiales Avanzados, Centro de Investigación en Química Aplicada (CIQA), Blvd. Enrique Reyna Hermosillo #140, Saltillo 25294, Coahuila, Mexico
- \* Correspondence: jroliva@conahcyt.mx

**Abstract:** In this study, we described the structural, morphological, optical, photoluminescence, and thermoluminescence properties of SrLaAlO<sub>4</sub>:Tm<sup>3+</sup>, Yb<sup>3+</sup> (SLAO:Tm,Yb) blue-emitting phosphors made by combustion synthesis and a post-annealing treatment at 1200 °C. The Yb co-dopant concentration was varied (1.0, 3.0, 5.0, and 6.0 mol%) while the Tm dopant concentration was fixed at 5 mol%. According to the X-ray diffraction patterns, all the samples presented the pure tetragonal phase of SrLaAlO<sub>4</sub>. Scanning electron microscopy analysis showed that the SLAO powders had morphologies of irregular or bar grains with average sizes in the range of 0.5–1.07 μm. Photoluminescence emission under 980 nm excitation showed an intense blue emission peak at 481 nm. The phosphors also emitted red light at 654 nm and a prominent NIR emission at 801 nm. All those emissions correspond to <sup>1</sup>G<sub>4</sub> → <sup>3</sup>H<sub>6</sub>, <sup>1</sup>G<sub>4</sub> → <sup>3</sup>H<sub>4</sub> and <sup>3</sup>H<sub>4</sub> → <sup>3</sup>H<sub>6</sub> transitions of Tm<sup>3+</sup>. The SLAO:Tm,Yb phosphors synthesized with 3.0 mol.% of the Yb co-dopant showed the highest emission intensity in the visible/near-infrared (NIR) range (400–800 nm), and its CIE coordinates corresponded to the blue color (0.19368, 0.15826). Additionally, thermoluminescence emissions were recorded for the SLAO:Tm,Yb phosphors. The samples were previously irradiated with UV wavelengths of 265 nm, 365 nm, and 385 nm prior to the thermoluminescent measurements. After this, the kinetic parameters such as frequency factors, activation energy (E), and order of kinetics were calculated using the Chen method. The thermoluminescent emissions demonstrated that the SLAO:Yb,Tm phosphors can be used for UV dosimetry.

**Keywords:** combustion synthesis; phosphor; strontium lanthanum aluminate; ytterbium; thulium; photoluminescence; thermoluminescence



**Citation:** Etafo, N.O.; Rodriguez Garcia, C.; Esquivel-Castro, T.A.; León-Madrid, M.I.; Santibañez, A.; Oliva, J. The Effect of a Yb Co-Dopant on the Blue Upconversion and Thermoluminescent Emission of SrLaAlO<sub>4</sub>:Yb<sup>3+</sup>, Tm<sup>3+</sup> Phosphors. *Coatings* **2023**, *13*, 1003. <https://doi.org/10.3390/coatings13061003>

Academic Editor: Peter P. Levin

Received: 30 March 2023

Revised: 20 May 2023

Accepted: 24 May 2023

Published: 28 May 2023



**Copyright:** © 2023 by the authors. Licensee MDPI, Basel, Switzerland. This article is an open access article distributed under the terms and conditions of the Creative Commons Attribution (CC BY) license (<https://creativecommons.org/licenses/by/4.0/>).

## 1. Introduction

The rare-earth-doped oxide phosphors have attracted wide interest in the last decades because they can produce several emission colors (blue, green, red, etc.) that can be used for lighting applications [1]. Those phosphors can be used in other applications such as solar cells, solid-state lasers, cell imaging, and drug delivery [1,2]. In addition, cooping the phosphors with thulium and ytterbium ions is useful to produce intense blue and near-infrared (NIR) emissions [2]. Some of the most efficient upconversion materials already reported for the production of blue emissions are NaYbF<sub>4</sub>:Tm<sup>3+</sup>, Yb<sup>3+</sup>, KY<sub>3</sub>F<sub>10</sub>:Tm<sup>3+</sup>, Yb<sup>3+</sup>,

and  $\text{Ca}_2\text{YbF}_7:\text{Tm}^{3+}$  [3–5]. However, such phosphors have some limitations such as (1) a loss of energy during the conversion of high-energy photons to low-energy photons. This also produces lower efficiency and quantum yield. (2) These materials are fluoride-based phosphors that can be chemically and thermally unstable in comparison with oxide-based phosphors [6,7]. Thus, it is necessary to develop other phosphors without these limitations. One promising candidate to overcome the disadvantages above is the strontium lanthanum aluminate ( $\text{SrLaAlO}_4$  or SLAO). This material presents a tetragonal structure in the Ruddlesden-popper phase and has a chemical formula of  $\text{ABCO}_4$  ( $\text{A}^{2+}$ —alkaline earth metal,  $\text{B}^{3+}$ —trivalent rare-earth, and  $\text{C}^{3+}$ —any metal) [8,9]. Sehrawat et al. studied the green emission (549 nm) of the  $\text{SrLaAlO}_4:\text{Er}^{3+}$  phosphor under UV excitation [10]. Additionally, white emission was achieved by exciting the  $\text{SrLaAlO}_4:\text{Dy}^{3+}$  system with 352 UV light [11]. In addition, an intense green emission was produced by  $\text{SrLaAlO}_4:\text{Yb}^{3+}$ ,  $\text{Er}^{3+}$  phosphors under infrared 980 nm excitation, and even more, a green LED was constructed using such phosphors [12]. In general, the  $\text{SrLaAlO}_4$  host is a potential candidate to be doped or co-doped with other rare earths to achieve light emission by the upconversion mechanism. Moreover, this material has high thermal, physical, and chemical stability [13–15]. There are scarce reports about rare-earth-doped  $\text{SrLaAlO}_4$  systems, and this system has not been doped with  $\text{Tm}^{3+}$  to the best of our knowledge. For this reason, we studied the emission (photoluminescent and thermoluminescent) properties of  $\text{SrLaAlO}_4:\text{Tm}^{3+}, \text{Yb}^{3+}$  (SLAO:Tm,Yb) in this research. We have successfully synthesized  $\text{SrLaAlO}_4:\text{Tm}^{3+}, \text{Yb}^{3+}$  phosphors by combustion synthesis. Some of the main findings were i) that the sample synthesized with 3.0 mol% of Yb produced the highest blue and near-infrared (NIR) emissions and ii) the strongest thermoluminescence was generated by the sample synthesized with 6 mol% of Yb. Overall, the results of this research demonstrated that the SLAO:Tm,Yb phosphors can be used for lighting applications or UV dosimetry.

## 2. Materials and Methods

### 2.1. Synthesis of $\text{SrLaAlO}_4$ and $\text{SrLaAlO}_4 : \text{Tm}, \text{Yb}$

The reagents for the preparation of the phosphors were purchased from Sigma Aldrich (St. Louis, MO, USA) and used as received: lanthanum nitrate hexahydrate ( $\text{La}(\text{NO}_3)_3 \cdot 6\text{H}_2\text{O}$ , (99.0%)), aluminum nitrate nonahydrate ( $\text{Al}(\text{NO}_3)_3 \cdot 9\text{H}_2\text{O}$  (98.0%)), strontium nitrate ( $\text{Sr}(\text{NO}_3)_2$  (99.0%)), thulium nitrate pentahydrate, ( $\text{Tm}(\text{NO}_3)_3 \cdot 5\text{H}_2\text{O}$  (99.99%)), ytterbium nitrate ( $\text{Yb}(\text{NO}_3)_3 \cdot 6\text{H}_2\text{O}$  (99.99%)), and urea ( $\text{CO}(\text{NH}_2)_2$  (99.0%)). The thulium concentration was fixed at 5 mol% in the  $\text{SrLaAlO}_4 : \text{Tm}, \text{Yb}$  (SLAO:Tm,Yb) phosphor, and the Yb dopant concentration was changed from 1 to 6 mol%. Those samples were named SLAO1, SLAO3, SLAO5, and SLAO6. Additionally, the undoped sample synthesized without dopants was prepared and labeled SLAO. A typical procedure for the synthesis of the  $\text{SrLaAlO}_4 : \text{Tm}, \text{Yb}$  phosphor was the following:  $6.76 \times 10^{-3}$  moles of lanthanum nitrate hexahydrate,  $7 \times 10^{-3}$  moles of aluminum nitrate nonahydrate,  $6.8 \times 10^{-3}$  moles of strontium nitrate,  $3 \times 10^{-5}$  moles of thulium nitrate pentahydrate,  $2 \times 10^{-5}$  moles of ytterbium nitrate hexahydrate, and  $4.5 \times 10^{-2}$  moles of urea were dissolved into 20 mL of deionized water and stirred for 20 min to obtain a homogenous solution. After this, the mixture solution was heated at 600 °C and the combustion synthesis occurred for 25 min. As a result, a fluffy powder was obtained. This powder was ground and finally annealed in air at 1200 °C for 6 h.

### 2.2. Characterization of $\text{SrLaAlO}_4$ and $\text{SrLaAlO}_4 : \text{Tm}, \text{Yb}$ Phosphors

The morphology of the SLAO:Tm,Yb samples and the undoped one was analyzed using scanning electron microscopy (JEOL ARM200F, Peabody, MA, USA) and an energy of 15 KV. The X-ray diffraction (XRD) patterns of the samples were obtained by using Bruker D8 equipment (Billerica, MA, USA) with a Cu-K $\alpha$  radiation ( $\lambda = 1.54056 \text{ \AA}$ ) in the  $2\theta$  range of 20–80°. Absorbance spectra of the SLAO and SLAO: Tm,Yb samples were acquired by using a UV-Vis Cary 5000 Agilent spectrophotometer (Santa Clara, CA, USA) in the range of 200–800 nm. The photoluminescence spectra of the phosphor samples were recorded

in the visible range by using a USB 65,000 Ocean Optics spectrophotometer (Peabody, MA, USA), and the excitation source was an IR Laser (CW, 980 nm, 1.6 W) from Besram Technologies (model 980MD-1.6W, Beijing, China). To perform the PL measurements under the same experimental conditions and to excite the same amount of powder, disk pellets with a 5 mm diameter and 100 mg of weight were made for each SLAO: Tm, Yb phosphor. To make such pellets, the powders for each sample were compacted using a mechanical press, and each pellet was positioned in the same position in the fluorometer to guarantee that each sample was excited by the NIR light under the same conditions. The lifetime curves were measured by using an Acton Pro SP3500i fluorometer coupled to an R955 photomultiplier tube (Hamamatsu, Shizuoka, Japan). In addition, the experimental setup included an SR 540 chopper (LA, CA, USA) and an oscilloscope Teledyne Lecroy (model LT 344). The frequency of the chopper was 33 Hz. The lifetime curves were recorded for the SLAO: Tm, Yb phosphors by exciting with an IR Laser (980 nm) at an emission wavelength of 481 nm. Thermoluminescence (TL) measurements were carried out by first exposing the SLAO, SLAO1, SLAO3, and SLAO6 phosphors to different UV lamps for 10 min. For this purpose, 3 different sources of UV radiation were employed: a UV-A LED lamp (385 nm, 10 W Chanzon Technology, Beijing, China), a UV-B light bulb (365 nm, 20 W Tecnolite, LA, CA, USA), and a UV-C fluorescence lamp (265 nm GC Wellness of 25 W, LA, CA, USA). After irradiating with UV light, the samples were placed on Harshaw 3500 equipment (Wisconsin, MA, USA) to obtain the thermoluminescence emission curves under the following conditions: 50 °C of preheat for 10 s, a heating rate of 10 °C/s, and a maximum heating temperature of 300 °C. The kinetic parameters were calculated using Chen's method. All the optical measurements were performed at room temperature.

### 3. Results and Discussion

#### 3.1. Structural and Morphological Characterization

Figure 1a shows a simulation of the crystalline structure of the SrLaAlO<sub>4</sub> host (made from VESTA), which consisted of octahedrons of AlO<sub>6</sub>, see the blue parts. The ionic radii of the atoms are Sr<sup>2+</sup> = 1.26 Å, La<sup>3+</sup> = 1.30 Å, and O<sup>2-</sup> = 1.24 Å [12]. The X-ray diffraction (XRD) patterns were obtained for the SLAO and SLAO: Tm, Yb samples synthesized with x = 1.0, 3.0, 5.0, and 6.0 mol.% of the Yb concentration, and are depicted in Figure 1b. It was observed that the samples have the tetragonal pure phase with diffracted peaks matching the pure SrLaAlO<sub>4</sub> (JCPDS #81-0744) [10–12]. The most intense diffraction peaks at 2θ = 24.9°, 2θ = 32.04°, and 2θ = 33.8° correspond to the (101), (103), and (110) orientations, respectively. The crystallite size for each sample of SLAO: Tm, Yb was calculated using the well-known Scherrer formula [10]:

$$D = \frac{K\lambda}{\beta \cos \theta} \quad (1)$$

where *K* is the shape factor (0.941), *λ* is the wavelength = 1.5418 Å (CuKα radiation), *β* is the full width at half maximum (FWHM), and *θ* is the diffraction angle observed from the (103) plane. The estimated values of the crystallite sizes were 8.832, 13.823, 12.717, 13.824, and 15.140 nm for the SLAO, SLAO1, SLAO3, SLAO5, and SLAO6 phosphors, respectively (see Table 1). In general, the crystallite size increases with the Yb concentration. In addition, diffraction peaks associated with impurities were not observed despite the high Yb concentration in the SLAO phosphors. The *a*, *b*, and *c* lattice parameters were also calculated using the diffraction peaks located at 2θ = 32.04°, 33.88°, and 48.72°, which corresponds to (103), (110), and (200) orientations, respectively. It can be noticed in Table 1 that the *a*, *b*, and *c* lattice parameters decrease as the Yb<sup>3+</sup> concentration increases from 1 to 5.0 mol%. The error (*ε*) was calculated for the *a*, *b*, and *c* lattice parameters in Table 1 and obtained values of *ε* = 0.12–0.4%. Moreover, the volume of the unit cell also decreases as the Yb<sup>3+</sup> concentration increases from 1 to 5 mol%. This agrees with the reports given by Jacob et al., where a diminution of the crystallite size occurred with the Tm concentration [16]. The radius percentage value (*D<sub>r</sub>*) was calculated for the dopant and

host ions. If  $D_r < 15\%$ , this means that the dopants are substituting the ion sites in the lattice without segregation of phases [14–16].

$$D_r = \frac{R_1(CN) - R_2(CN)}{R_1(CN)} \times 100\% \quad (2)$$

where  $R_1(CN)$  and  $R_2(CN)$  are assigned to the radii of the substituted ions ( $\text{Sr}^{2+}$  or  $\text{La}^{3+}$ ) and dopant ions ( $\text{Yb}^{3+}$  or  $\text{Tm}^{3+}$ ), respectively. They have ionic radii and coordinate numbers (CN) as follows:  $\text{Sr}^{2+} = 1.26 \text{ \AA}$  (CN = 8),  $\text{La}^{3+} = 1.16 \text{ \AA}$  (CN = 8),  $\text{Yb}^{3+} = 0.985 \text{ \AA}$  (CN = 8), and  $\text{Tm}^{3+} = 0.994 \text{ \AA}$  (CN = 8). The estimated value of  $D_r$  between the  $\text{Yb}^{3+}$  and  $\text{La}^{3+}$  ions was 13.07%, while the  $D_r$  value for the  $\text{Tm}^{3+}$  and  $\text{La}^{3+}$  ions was 12.23%. As observed, the values of  $D_r$  were below 15%. This indicates that both the  $\text{Yb}^{3+}$  and  $\text{Tm}^{3+}$  ions are substituting the  $\text{La}^{3+}$  ions in the  $\text{SrLaAlO}_4$  system [17].

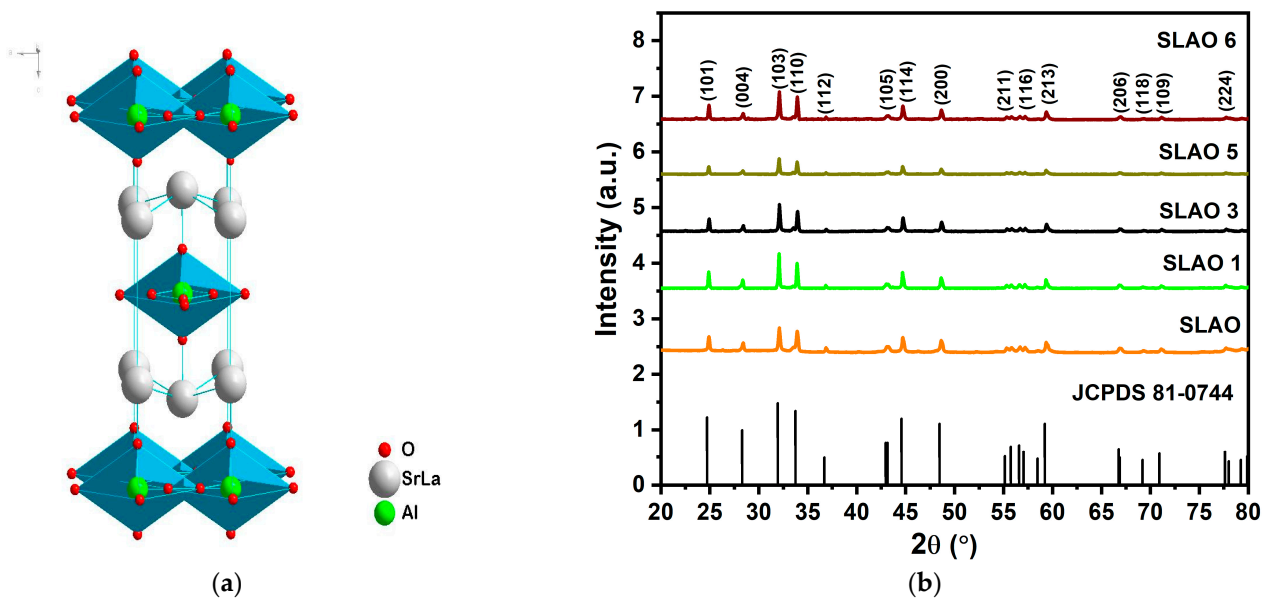


**Figure 1.** (a) A visualization of the crystalline structure of the pure tetragonal  $\text{SrLaAlO}_4$ . The green, red, and gray spheres correspond to Al, O, and Sr/La atoms, respectively. The blue color shows  $\text{AlO}_4$  octahedrons. (b) X-ray diffraction patterns of the pure  $\text{SrLaAlO}_4$  and  $\text{SrLaAlO}_4:\text{Tm,Yb}$  phosphors.

**Table 1.** The volume and crystallite size of the  $\text{SLAO}:\text{Tm,Yb}$  phosphors at different co-dopant concentrations of Yb with fixed  $\text{Tm} = 5 \text{ mol}\%$  dopant concentration.

Sample	a (Å)	b (Å)	c (Å)	Volume (Å <sup>3</sup> )	Crystallite Size (nm)
SLAO	3.7504	3.7504	12.669	178.196	17.38
SLAO1	3.7377	3.7377	12.615	176.991	16.95
SLAO3	3.7435	3.7435	12.600	176.574	14.22
SLAO5	3.7433	3.7433	12.541	175.728	13.04
SLAO6	3.7435	3.7435	12.517	176.411	12.02

The SEM images in Figure 2 show the morphology of the SLAO, SLAO1, SLAO3, and SLAO6 phosphors. The average size of the  $\text{SLAO}:\text{Tm,Yb}$  phosphors was determined from the SEM images, and we employed Image J software. The average particle size for each sample was calculated by averaging the sizes of 200–300 microparticles. We also calculated the particle size distribution for each sample, see Figure S1 in the Supporting Information. Figure 2a shows the SEM image for the pure SLAO (undoped host). We observe coalesced particles with irregular shapes and sizes of 0.3–1  $\mu\text{m}$ . If the concentration of the  $\text{Yb}^{3+}$  dopant is incremented to 1.0 mol% (SLAO1), it now observes particles of



irregular shapes mixed with micro-rods; see the green circles in Figure 2b. The average length of the bars was 1  $\mu\text{m}$ . The SLAO3 phosphor shows mostly micro-rods with an average length size of 0.68  $\mu\text{m}$  and an average width of 0.15  $\mu\text{m}$  (see the orange circles in Figure 2c). Some irregular particles are also observed with an average size of 0.93  $\mu\text{m}$ . Moreover, the SLAO6 phosphor made with 6 mol% of Yb showed a high agglomeration of particles, and the micro-rods disappeared, as seen in Figure 2d, see the blue circle. Overall, the SEM results demonstrate that raising the co-dopant concentration of  $\text{Yb}^{3+}$  increases the coalescence degree of the SLAO: Tm,Yb microparticles. This phenomenon has been observed in previous rare-earth-doped oxide phosphors [18]. Possibly, an imbalance of charges occurred at higher  $\text{Yb}^{3+}$  concentrations, which avoids the formation of particles with well-defined morphology [18].

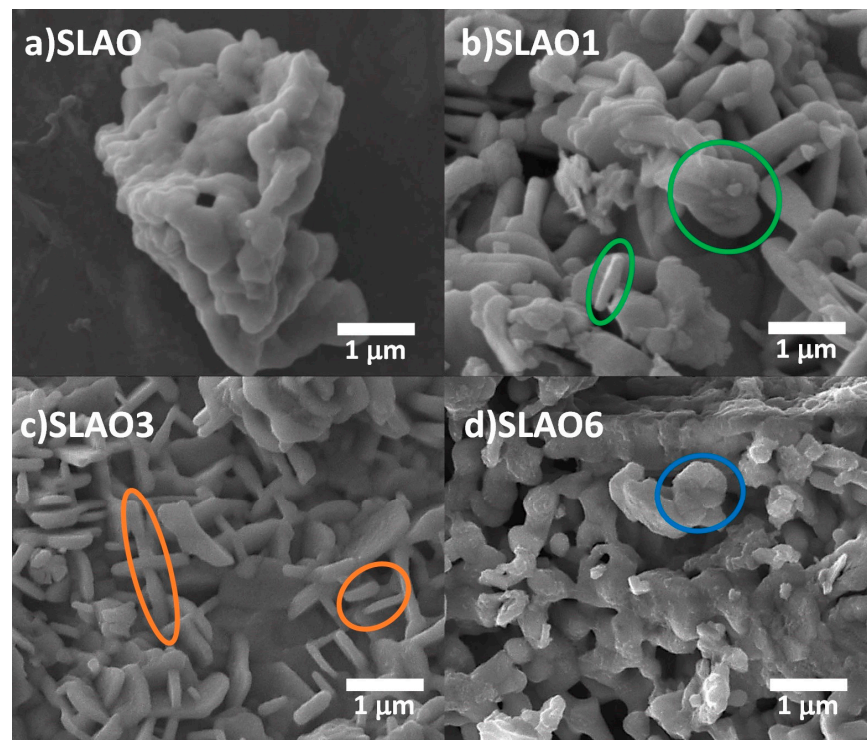


**Figure 2.** SEM micrographs for the (a) pure/undoped  $\text{SrLaAlO}_4$ , (b) SLAO1, (c) SLAO3, and (d) SLAO6 phosphors.

### 3.2. Absorbance and Optical Band Gap of the $\text{SrLaAlO}_4$ and $\text{SrLaAlO}_4:\text{Tm, Yb}$ Phosphors

The absorbance spectrum of the undoped SLAO phosphor (see Figure 3a) shows a UV absorption band at 230 nm (edge band gap absorption). The absorbance spectra of SLAO:Tm,Yb exhibits a peak at 318 nm, which is attributed to the  $^1D_2 \rightarrow ^3H_6$  transition of  $\text{Tm}^{3+}$  [19,20]. Additionally, the intensity of the band at 318 nm increases with the Yb concentration, which is consistent with the energy transfer from the Yb sensitizer to the Tm ions [19,20]. The optical band gap values for both the undoped SLAO and SLAO1–SLAO6 phosphors were calculated from the absorbance spectra using the well-known Tauc plot procedure, which provides plots of  $(\alpha h\nu)^{1/n}$  vs. energy (eV). The band gap is obtained from those curves by intersecting the linear section with the energy axis ( $\alpha h\nu = 0$ ), as seen in Figure 3b.  $\alpha$  is the absorption coefficient,  $h\nu$  is the photon energy,  $h$  is the plank constant, and  $\nu$  is the frequency of light.  $n$  was taken as  $\frac{1}{2}$  because  $\text{SrLaAlO}_4$  is a direct band gap material [21]. The optical band decreased with the Yb concentration from 1 to 6 mol%, as seen in Figure 3b. The pure host has a band gap value of 5.06 eV. Furthermore, the refractive indexes of the phosphors were calculated using the following formula [22]:

$$\frac{n^2 - 1}{n^2 + 1} = 1 - \sqrt{\frac{\epsilon_g}{20}}, \quad (3)$$

where  $n$  = the refractive index and  $\epsilon_g$  = optical band, and we obtained a refractive index of 1.725, 1.734, 1.736, 1.738, and 1.741 for the SLAO, SLAO1, SLAO3, SLAO5, and SLAO6 phosphors, respectively. As the concentration of Yb increases in the SLAO host, the refractive index generally increases, and this reduces the scattering loss of light. This agrees with the report of Xu et al., who reported that the refractive index of an efficient phosphor is 1.83. In our case, we obtained refractive indexes close to 1.83; thus, we should have a low scattering of light, and this contributes to the enhancement of photoluminescence [23].

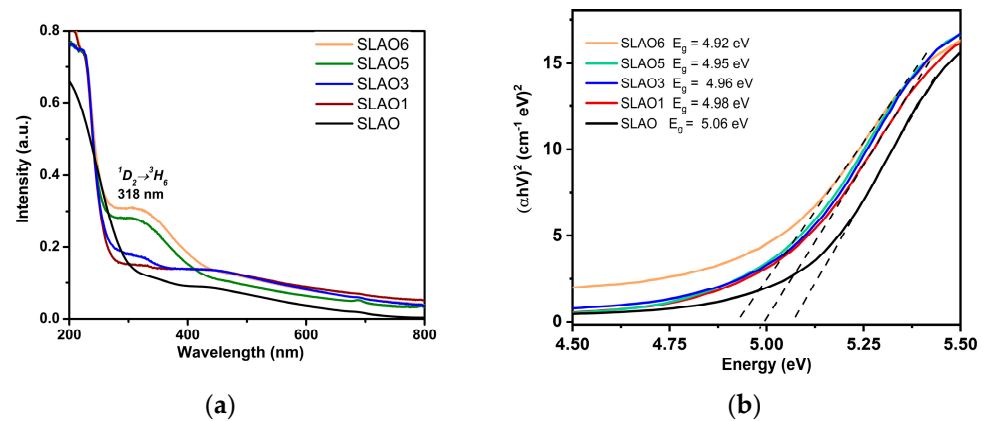


**Figure 3.** (a) Absorbance spectra and (b) Tauc plot for the undoped SrLaAlO<sub>4</sub> and SrLaAlO<sub>4</sub>:Tm, Yb phosphors.

### 3.3. Upconversion Luminescent Emission of the SLAO:Tm, Yb Phosphors

Figure 4a shows the upconversion emission of the SrLaAlO<sub>4</sub>:Tm,Yb phosphors (under 980 nm excitation). It is observed at an emission of 801 nm ( $^3H_4 \rightarrow ^3H_6$  transition), 481 nm ( $^1G_4 \rightarrow ^3H_6$  transition), and 654 nm ( $^1G_4 \rightarrow ^3H_4$ ) [23,24]. Both the visible and NIR emissions increase with the Yb<sup>3+</sup> concentration (up to 3.0 mol%) and decrease for Yb concentrations above 5 mol%. The decrease in the emission intensity at high Yb concentrations (7 mol%) has been observed in the BaLaAlO<sub>4</sub>:Tm<sup>3+</sup>,Yb<sup>3+</sup>, and Sr<sub>2</sub>CeO<sub>4</sub>:Yb<sup>3+</sup>,Tm<sup>3+</sup> systems [25,26]. In our case, the emission decreased after 5 mol% due to the quenching concentration effect, which consisted of the continuous re-absorption of energy among the Yb ions (this avoided the generation of emission photons) [27]. In fact, we found in the literature that the systems of Lu<sub>2</sub>O<sub>3</sub>:X-mol%Yb<sup>3+</sup>, 0.2 mol%Tm<sup>3+</sup> (X from 0 to 15 mol%) and CaMoO<sub>4</sub>:X-mol%Yb<sup>3+</sup>, 0.5 mol%Tm<sup>3+</sup> (X from 0 to 20 mol%) suffered the quenching of luminescence as the Yb concentration increased [28,29]. According to the articles for those last systems, emission quenching occurred because the distance between the dopant ion decreases, allowing non-radiative energy transfer among dopants (multipole–multipole interactions). On the other hand, the contribution of the different emission colors to the total emission was calculated. For the SLAO1–SLAO6 samples, the blue emission represents 2.28%–30.12% of the overall visible emission in the spectrum. Additionally, the red emission contributes 6.134%–11.24% of the overall emission spectra. The NIR emission represents 14.69%–58.63% of the overall emission. The emission intensity decreased in the following order: NIR > blue > red because the  $^3H_4 \rightarrow ^3H_6$  transition is mainly favored after the energy transfer from the Yb<sup>3+</sup> to the Tm<sup>3+</sup>. Consequently, fewer electrons are available to be recombined for the generation of photons; this, in turn, produces weaker blue/red emissions [30–32]. In fact, strong NIR emission is useful for applications, such as bio-imaging and cell labeling [33]. The inset in Figure 4a shows a photograph of the blue emission produced by the SLAO3 sample (made with Tm<sup>3+</sup> = 5 mol%, and Yb<sup>3+</sup> = 3.0 mol%) under 980 nm excitation (0.5 W of power). The photograph was taken in darkness using an IR filter (cutoff wavelength = 850 nm). Figure 4b shows the integrated NIR emission (at 801 nm) as a function of the Yb concentration. The maximum emission was produced by the sample synthesized with 3 mol% of Yb<sup>3+</sup>.

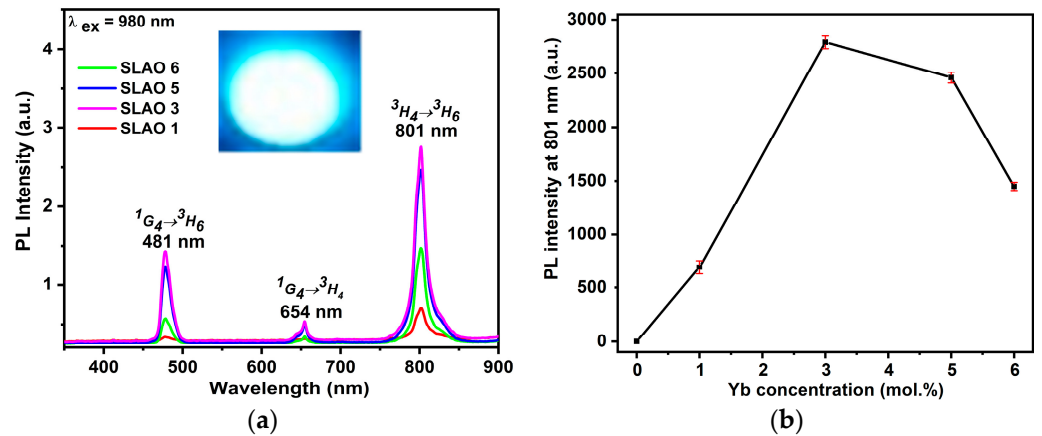


**Figure 4.** (a) Upconversion spectra of the SrLaAlO<sub>4</sub>:Tm,Yb phosphors and (b) PL intensity (at 801 nm) as a function of the Yb concentration of SrLaAlO<sub>4</sub>:Tm, Yb phosphors. The inset is a photograph of the blue emission of the SLAO3 phosphors.

The lifetime curves of the SrLaAlO<sub>4</sub>: Tm,Yb phosphors are presented in Figure S2 of the Supporting Information. We use the following equation:  $I = I_0 \exp(-t/\tau)$ , where  $I$  is the PL intensity at time  $t$ ,  $I_0$  is the intensity at time  $t = 0$ , and  $\tau$  is the lifetime. The values of the lifetime (at  $\lambda_{\text{emis}} = 481$  nm) were 61, 68, 105  $\mu\text{s}$ , and 184  $\mu\text{s}$  for the SLAO1, SLAO3, SLAO5, and SLAO6, respectively. As observed, the lifetime increased with the Yb concentration, and this occurred because more defects were formed in the host matrix as the Yb concentration increased which, in turn, delayed the photoluminescent emission of Tm<sup>3+</sup> (the defects worked as electron trapping centers that delayed the electron-hole recombination, which caused the emission of light) [34,35]. The increase in the lifetime with the Yb concentration (at fixed Tm<sup>3+</sup> concentration and  $\lambda_{\text{emis}} = 475$  nm) was also observed in the systems of SiO<sub>2</sub>-CaO:X-mol%Yb<sup>3+</sup>, 0.15 mol%Tm<sup>3+</sup> (X from 1 to 4 mol%) and GdVO<sub>4</sub>:X-mol%Yb<sup>3+</sup>, 3 mol%Tm<sup>3+</sup> (X from 0 to 9 mol%) [36,37].

The Commission International de l’Eclairage (CIE) color coordinates were calculated from the PL emission spectra of SLAO:Tm, Yb phosphors, as seen in Figure 5. The color coordinates were (0.21824, 0.17945), (0.19368, 0.15826), (0.22078, 0.20033), and (0.19624, 0.16416) for the SLAO1, SLAO3, SLAO5, and SLAO6. All those coordinates are located in the blue region of the CIE map.

**CIE 1931**

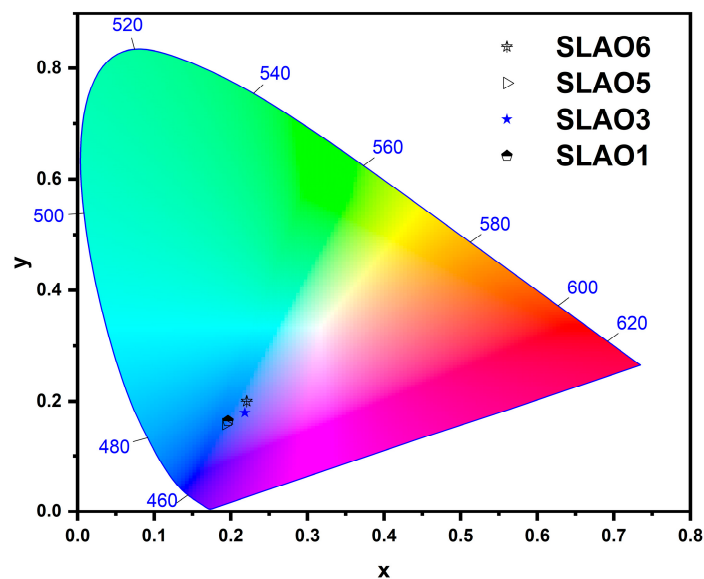


**Figure 5.** A CIE color map for the PL spectra of the SrLaAlO<sub>4</sub>:Tm, Yb phosphors.

### 3.4. The TL Emission of the SLAO:Tm,Yb Phosphors

Thermoluminescence (TL) properties of the SLAO, SLAO1, SLAO3, and SLAO6 phosphors were studied. Firstly, the phosphors were exposed to different UV sources (265 or 365, or 385 nm) for 10 min to create traps in the samples. After UV irradiation, the samples were heated in the range of 50 °C–300 °C to release the electrons confined in the traps of the samples. TL spectra of the SLAO, SLAO1, SLAO3, and SLAO6 samples after irradiation with a 385 nm source are presented in Figure 6a. The TL signal presents two main peaks, one around 125 °C and the second around 250 °C–260 °C. The most intense TL response was obtained for the SLAO6 sample. Since the TL emission is proportional to the content of defects in the samples, the SLAO6 sample should have the highest content of defects [38–41]. The TL response of the SLAO, SLAO1, SLAO3, and SLAO6 samples (previously irradiated with 365 nm) is shown in Figure 6b. In this plot, the SLAO and SLAO1 samples present a weaker emission in comparison with the SLAO3 sample, which exhibited a wide peak at 160 °C. The most intense TL emission is also obtained for the SLAO6 sample, which reveals a prominent peak band at 250 °C. This peak could be due to the intrinsic effects of the crystal lattice rather than new defects or color centers induced by the higher Yb concentration [42,43]. Figure 6c shows TL responses of the SLAO, SLAO1, SLAO3, and SLAO6 samples after 265 nm irradiation. Irradiation with this last UV wavelength produced higher TL emissions than the 385 nm and 365 nm wavelengths. Moreover, the undoped SLAO sample presents a weak TL response. The SLAO1 sample shows a weak TL band in the range of 140–180 °C, while the SLAO3 and SLAO6 samples show TL peaks at 160 °C and 140 °C [44–46], respectively. Previous reports in the literature about the TL properties of phosphors doped with Yb demonstrated that the introduction of Yb ions into the lattice sites caused the formation of oxygen vacancies, which act like electron traps with high activation energy [44–47]. Thus, the SLAO6 sample, which presented the highest TL emission, should have the highest content of oxygen vacancy defects.

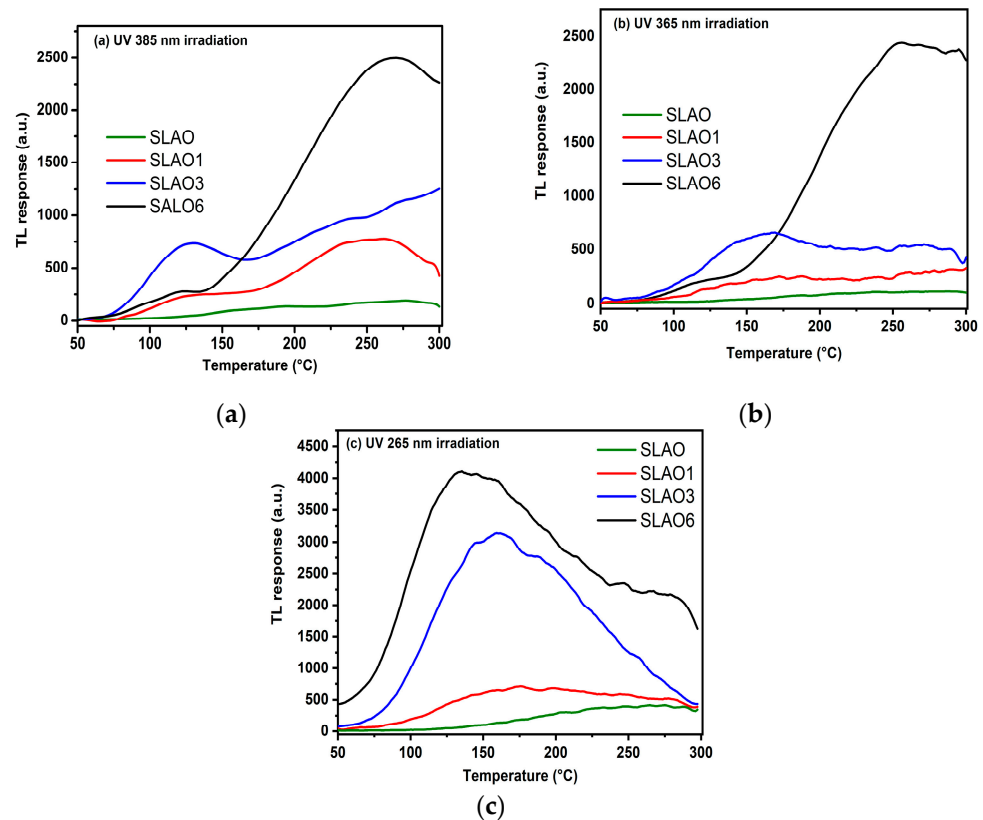


**Figure 6.** TL emission spectra of the undoped SrLaAlO<sub>4</sub> sample and the SrLaAlO<sub>4</sub>:Tm, Yb phosphors after irradiation with different ultraviolet lamps: (a) 385 nm, (b) 365 nm, and (c) 265 nm.



Kinetic parameters were calculated for the TL response obtained from the SLAO:Tm,Yb samples previously irradiated with 265 nm, as seen in Table 2. This one shows the kinetic order tendency, activation energy, and frequency factor, which were calculated employing Chen's method [48]. The activation energy represents the position of the trapping level within the forbidden gap, while the frequency factor represents the number of times that the electrons interact with the trapping centers before the recombination of the electron holes, which produce the TL emission. In addition, it can be appreciated that the activation energy (E) shown in Table 2 is consistent in all samples; peak 1 is around 0.5 eV in almost all samples while peak 2 is around 0.4 eV but the frequency factor increases as the Yb increases. This allows the process of recombination and re-trapping of the electrons in the host SrLaAlO<sub>4</sub> matrix.

**Table 2.** Kinetic parameters for the TL emission of the SLAO and SLAO:Tm,Yb samples (under 265 nm excitation).

	PEAK	Activation Energy, E (eV)	Frequency Factor (S) (S−1)
SLAO6	1	0.566	$8.68 \times 10^6$
	2	0.429	$1.84 \times 10^4$
	3	0.689	$9.26 \times 10^5$
SLAO3	1	0.616	$1.26 \times 10^7$
	2	0.424	$1.05 \times 10^4$
SLAO1	1	0.549	$1.15 \times 10^6$
	2	0.414	$2.80 \times 10^3$
SLAO	1	0.446	$6.48 \times 10^3$

#### 4. Conclusions

In this work, we reported a simple combustion synthesis to synthesize SrLaAlO<sub>4</sub>:Tm,Yb phosphors. The XRD analysis demonstrated that the undoped SLAO and SLAO:Tm,Yb samples presented a tetragonal phase. SEM images demonstrated that the SLAO:Tm,Yb samples increased their coalescence degree as the concentration of Yb in the SLAO host increased. Another effect was the diminution of the crystallite size when the Yb concentration increased from 1 to 5 mol%. The highest luminescent intensity produced in the visible/near-infrared (NIR) range (400–800 nm) was obtained for the sample doped with 3 mol% of Yb. The upconversion emission of the SLAO:Tm,Yb samples showed emissions at 481 nm, 654 nm, and 801 nm under 980 nm excitation. Moreover, the most intense TL emission was obtained in the SLAO6 sample previously irradiated with 265 nm. In general, any SLAO sample irradiated with UV light generated a TL signal. This suggests that the SLAO phosphors can be used for dosimeter applications.

**Supplementary Materials:** The following supporting information can be downloaded at: <https://www.mdpi.com/article/10.3390/coatings13061003/s1>, Figure S1: Histograms for SLAO:Yb,Tb particles; Figure S2: Decay time curves for the SLAO:Yb,Tb particles.

**Author Contributions:** Conceptualization; methodology, software, and validation—N.O.E.; writing—review and editing and resources—C.R.G.; formal analysis and investigation—T.A.E.-C.; formal analysis and investigation—M.I.L.-M.; visualization, supervision, and project administration—A.S.; writing—review and editing, visualization, supervision, and project administration—J.O. All authors have read and agreed to the published version of the manuscript.

**Funding:** Conahcyt, Mexico, Grant Number: 1110994.

**Institutional Review Board Statement:** Not applicable.

**Informed Consent Statement:** Not applicable.

**Data Availability Statement:** Not applicable.

**Acknowledgments:** N.O. Etafo acknowledges CONAHCYT-Mexico for the Ph.D. scholarship 1110994. The authors acknowledge Luis Armando Díaz Torres and Eduardo Montes Ramírez from the Centro de Investigaciones en Óptica A.C. and the Universidad de Guanajuato for the measurements of the decay time. We appreciate the support from the LANIAUTO and LNMG laboratories.

**Conflicts of Interest:** The authors declare that they have no competing financial interest or personal relationships that could have appeared to influence the work reported in this paper.

## References

1. Liu, B.-M.; Gan, W.-J.; Lou, S.-Q.; Zou, R.; Tang, Q.; Wang, C.-X.; Jiao, J.; Wang, J. X-ray-activated, UVA persistent luminescent materials based on Bi-doped SrLaAlO<sub>4</sub> for deep-Seated photodynamic activation. *J. Appl. Phys.* **2021**, *129*, 120901. [[CrossRef](#)]
2. Pirri, A.; Maksimov, R.N.; Li, J.; Vannini, M.; Toci, G. Achievements and Future Perspectives of the Trivalent Thulium-Ion-Doped Mixed-Sesquioxide Ceramics for Laser Applications. *Materials* **2022**, *15*, 2084. [[CrossRef](#)]
3. Gao, W.; Ge, W.; Shi, J.; Chen, X.; Li, Y. A novel upconversion optical thermometers derived from non-thermal coupling levels of CaZnOS:Tm/Yb phosphors. *J. Solid State Chem.* **2021**, *297*, 122063. [[CrossRef](#)]
4. Lv, S.; Zhang, K.; Zhu, L.; Tang, D. ZIF-8-Assisted NaYF<sub>4</sub>:Yb,Tm@ZnO Converter with Exonuclease III-Powered DNA Walker for Near-Infrared Light Responsive Biosensor. *Anal. Chem.* **2019**, *92*, 1470–1476. [[CrossRef](#)]
5. Saidi, K.; Dammak, M.; Soler-Carracedo, K.; Martín, I.R. A novel optical thermometry strategy based on emission of Tm<sup>3+</sup>/Yb<sup>3+</sup> codoped Na<sub>3</sub>GdV<sub>2</sub>O<sub>8</sub> phosphors. *Dalton Trans.* **2022**, *51*, 5108–5117. [[CrossRef](#)] [[PubMed](#)]
6. Lei, Y.; Li, Y.; Jin, Z. Photon energy loss and management in perovskite solar cells. *Energy Rev.* **2022**, *1*, 100003. [[CrossRef](#)]
7. Datt, R.; Bishnoi, S.; Hughes, D.; Mahajan, P.; Singh, A.; Gupta, R.; Arya, S.; Gupta, V.; Tsoi, W.C. Downconversion Materials for Perovskite Solar Cells. *Sol. RRL* **2022**, *6*, 2200266. [[CrossRef](#)]
8. Lin, Z.-L.; Zeng, H.-J.; Zhang, G.; Xue, W.-Z.; Pan, Z.; Lin, H.; Loiko, P.; Liang, H.-C.; Petrov, V.; Mateos, X.; et al. Kerr-lens mode-locked Yb:SrLaAlO<sub>4</sub> laser. *Opt. Express* **2021**, *29*, 42837. [[CrossRef](#)]
9. Petit, P.; Petit, J.; Goldner, P.; Viana, B. Inhomogeneous broadening of optical transitions in Yb:CaYAlO<sub>4</sub>. *Opt. Mater.* **2008**, *30*, 1093–1097. [[CrossRef](#)]
10. Sehwat, P.; Khatkar, A.; Boora, P.; Hooda, A.; Kumar, M.; Malik, R.K.; Khatkar, S.P.; Taxak, V.B. A novel strategy for high color purity virescent Er<sup>3+</sup>-doped SrLaAlO<sub>4</sub> nanocrystals for solid-state lighting applications. *J. Mater. Sci. Mater. Electron.* **2020**, *31*, 6072–6083. [[CrossRef](#)]
11. Sehwat, P.; Khatkar, A.; Boora, P.; Kumar, M.; Malik, R.; Khatkar, S.; Taxak, V. Emanating cool white light emission from novel down-converted SrLaAlO<sub>4</sub>:Dy<sup>3+</sup> nanophosphors for advanced optoelectronic applications. *Ceram. Int.* **2020**, *46*, 16274–16284. [[CrossRef](#)]
12. Garcia, C.R.; Oliva, J.; Carranza, J.; Mtz-Enriquez, A.I.; Hdz-Garcia, H.M.; Santibañez, A.; Chavez, D. Green Upconversion of a SrLaAlO<sub>4</sub>:Yb,Er Phosphor and Its Application for LED Illumination. *J. Electron. Mater.* **2022**, *52*, 1357–1365. [[CrossRef](#)]
13. Loiko, P.; Druon, F.; Georges, P.; Viana, B.; Yumashev, K. Thermo-optic characterization of Yb:CaGdAlO<sub>4</sub> laser crystal. *Opt. Mater. Express* **2014**, *4*, 2241–2249. [[CrossRef](#)]
14. Huang, X.; He, C.; Wen, X.; Huang, Z.; Liu, Y.; Fang, M.; Wu, X.; Min, X. Preparation, structure, luminescence properties of terbium doped perovskite-like structure green-emitting phosphors SrLaAlO<sub>4</sub>:Tb<sup>3+</sup>. *Opt. Mater.* **2019**, *95*, 109191. [[CrossRef](#)]
15. Sankarasubramanian, K.; Devakumar, B.; Annadurai, G.; Sun, L.; Zeng, Y.-J.; Huang, X. Novel SrLaAlO<sub>4</sub>:Mn<sup>4+</sup> deep-red emitting phosphors with excellent responsiveness to phytochrome P<sub>FR</sub> for plant cultivation LEDs: Synthesis, photoluminescence properties, and thermal stability. *RSC Adv.* **2018**, *8*, 30223–30229. [[CrossRef](#)]
16. Jacob, L.A.; Sisira, S.; Mani, K.P.; Thomas, K.; Alexander, D.; Biju, P.; Unnikrishnan, N.; Joseph, C. High purity blue photoluminescence in thulium activated α-Na<sub>3</sub>Y(VO<sub>4</sub>)<sub>2</sub> nanocrystals via host sensitization. *J. Lumin.* **2020**, *223*, 117169. [[CrossRef](#)]
17. Hua, Y.; Yu, J.S. Warm white emission of LaSr<sub>2</sub>F<sub>7</sub>:Dy<sup>3+</sup>/Eu<sup>3+</sup> NPs with excellent thermal stability for indoor illumination. *J. Mater. Sci. Technol.* **2020**, *54*, 230–239. [[CrossRef](#)]
18. Etafo, N.; Oliva, J.; Garcia, C.; Mtz-Enriquez, A.; Ruiz, J.; Avalos-Belmontes, F.; Lopez-Badillo, C.; Gomez-Solis, C. Enhancing of the blue/NIR emission of novel BaLaAlO<sub>4</sub>:Yb<sup>3+</sup>(X mol%),Tm<sup>3+</sup>(0.5 mol%) upconversion phosphors with the Yb<sup>3+</sup> concentration (X = 0.5 to 6). *Inorg. Chem. Commun.* **2022**, *137*, 109192. [[CrossRef](#)]
19. Huang, C.-H.; Chen, T.-M.; Cheng, B.-M. Luminescence Investigation on Ultraviolet-Emitting Rare-Earth-Doped Phosphors Using Synchrotron Radiation. *Inorg. Chem.* **2011**, *50*, 6552–6556. [[CrossRef](#)]
20. Pisarski, W.A.; Pisarska, J.; Lisiecki, R.; Ryba-Romanowski, W. Broadband Near-Infrared Luminescence in Lead Germanate Glass Triply Doped with Yb<sup>3+</sup>/Er<sup>3+</sup>/Tm<sup>3+</sup>. *Materials* **2021**, *14*, 2901. [[CrossRef](#)]
21. Yue, C.; Pu, Y.; Zhu, D.; Yan, Q. A novel green-emitting SrLaAlO<sub>4</sub>:Er<sup>3+</sup> phosphor synthesized by co-precipitation method for w-LEDs and optical thermometry. *J. Mater. Sci. Mater. Electron.* **2021**, *32*, 4228–4238. [[CrossRef](#)]
22. Xu, X.; Li, H.; Zhuo, Y.; Xiong, D.; Chen, M. Gradient refractive index structure of phosphor-in-glass coating for packaging of white LEDs. *J. Am. Ceram. Soc.* **2018**, *102*, 1677–1685. [[CrossRef](#)]
23. Goud, K.; Ramesh, C.; Rao, A. Spectroscopic Properties and Energy Transfer in Lead Bismuth Gallium Borate Glasses Codoped with Tm<sup>3+</sup> and Yb<sup>3+</sup>. *Int. J. Eng. Res. Technol.* **2017**, *6*, 2278-0181. [[CrossRef](#)]

24. Zhang, Y.; Wang, Y.; Deng, J.; Wang, J.; Ni, S. Highly efficient Yb<sup>3+</sup>/Tm<sup>3+</sup> co-doped NaYF<sub>4</sub> nanotubes: Synthesis and intense ultraviolet to infrared up-conversion luminescence. *Opt. Commun.* **2014**, *312*, 43–46. [[CrossRef](#)]
25. Etafo, N.O.; Carranza, J.O.; Garcia, C.E.R.; Oliva, J.; Viesca-Villanueva, E.; Hernández-Hernández, E.; Santibañez, A.; Gomez-Zavala, O. Blue/NIR-emitting Phosphor Based on Sr<sub>2</sub>CeO<sub>4</sub>: Tm<sup>3+</sup>, Yb<sup>3+</sup> Obtained by Combustion Synthesis. *Mater. Sci.* **2023**, 1–6, *in press*. [[CrossRef](#)]
26. Dan, H.K.; Tap, T.D.; Vinh, H.X.; Ty, N.M.; Vinh, L.; Zhou, D.; Qiu, J. Enhanced red upconversion emission and energy transfer of Tm<sup>3+</sup>/Cr<sup>3+</sup>/Yb<sup>3+</sup> tri-doped transparent fluorosilicate glass-ceramics. *J. Non-Crystalline Solids* **2020**, *535*, 119885. [[CrossRef](#)]
27. Wang, Z.; Meijerink, A. Concentration Quenching in Upconversion Nanocrystals. *J. Phys. Chem. C* **2018**, *122*, 26298–26306. [[CrossRef](#)]
28. Li, L.; Lin, H.; Zhao, X.; Wang, Y.; Zhou, X.; Ma, C.; Wei, X. Effect of Yb<sup>3+</sup> concentration on upconversion luminescence in Yb<sup>3+</sup>, Tm<sup>3+</sup> co-doped Lu<sub>2</sub>O<sub>3</sub> nanophosphors. *J. Alloy Compd.* **2013**, *586*, 555–560. [[CrossRef](#)]
29. Chung, J.H.; Ryu, J.H.; Lee, S.Y.; Kang, S.H.; Shim, K.B. Effect of Yb<sup>3+</sup> and Tm<sup>3+</sup> concentrations on blue and NIR upconversion luminescence in Yb<sup>3+</sup>, Tm<sup>3+</sup> co-doped CaMoO<sub>4</sub>. *Ceram. Int.* **2012**, *39*, 1951–1956. [[CrossRef](#)]
30. Zheng, W.; Huang, P.; Tu, D.; Ma, E.; Zhu, H.; Chen, X. Lanthanide-doped upconversion nano-bioprobes: Electronic structures, optical properties, and biodetection. *Chem. Soc. Rev.* **2014**, *44*, 1379–1415. [[CrossRef](#)]
31. Li, Z.; Zhang, Y.; La, H.; Zhu, R.; El-Banna, G.; Wei, Y.; Han, G. Upconverting NIR Photons for Bioimaging. *Nanomaterials* **2015**, *5*, 2148–2168. [[CrossRef](#)] [[PubMed](#)]
32. Kumari, A.; Rai, V.K. NIR to blue light upconversion in Tm<sup>3+</sup>/Yb<sup>3+</sup> codoped BaTiO<sub>3</sub> tellurite glass. *AIP Conf. Proc.* **2015**, *1661*, 100006. [[CrossRef](#)]
33. Baldacchini, G.; Davidson, A.T.; Kalinov, V.S.; Kozakiewicz, A.G.; Montekali, R.M.; Nichelatti, E.; Voitovich, A.P. Thermoluminescence of pure LiF crystals and color centers. *J. Lumin.* **2007**, *122–123*, 371–373. [[CrossRef](#)]
34. Pathak, N.; Sanyal, B.; Gupta, S.K.; Kadam, R.M. MgAl<sub>2</sub>O<sub>4</sub> both as short and long persistent phosphor material: Role of antisite defect centers in determining the decay kinetics. *Solid State Sci.* **2018**, *88*, 13–19. [[CrossRef](#)]
35. Ding, J.; Lian, Z.; Li, Y.; Wang, S.; Yan, Q. The Role of Surface Defects in Photoluminescence and Decay Dynamics of High-Quality Perovskite MAPbI<sub>3</sub> Single Crystals. *J. Phys. Chem. Lett.* **2018**, *9*, 4221–4226. [[CrossRef](#)]
36. Gavrilović, T.V.; Nikolic, M.; Jovanović, D.J.; Dramićanin, M.D. Up-conversion luminescence of Tm<sup>3+</sup> sensitized by Yb<sup>3+</sup> ions in GdVO<sub>4</sub>. *Phys. Scr.* **2013**, *T157*, 014055. [[CrossRef](#)]
37. Halubek-Gluchowska, K.; Szymański, D.; Tran, T.N.L.; Ferrari, M.; Lukowiak, A. Upconversion Luminescence of Silica–Calcium Nanoparticles Co-doped with Tm<sup>3+</sup> and Yb<sup>3+</sup> Ions. *Materials* **2021**, *14*, 937. [[CrossRef](#)]
38. Mayhugh, M.R.; Christy, R.W.; Johnson, N.M. Thermoluminescence and Color Center Correlations in Dosimetry LiF. *J. Appl. Phys.* **1970**, *41*, 2968–2976. [[CrossRef](#)]
39. Pérez-Cruz, L.; Cruz-Zaragoza, E.; Díaz, D.; Alcántara, J.H.; García, E.C.; Sánchez, H.M. Synthesis, optical and thermoluminescence properties of thulium-doped KMgF<sub>3</sub> fluoroperovskite. *Appl. Radiat. Isot.* **2021**, *177*, 109913. [[CrossRef](#)]
40. Roman-Lopez, J.; Correcher, V.; Garcia-Guinea, J.; Rivera, T.; Lozano, I. Cathodoluminescence and green-thermoluminescence response of CaSO<sub>4</sub>:Dy,P films. *J. Lumin.* **2013**, *135*, 89–92. [[CrossRef](#)]
41. Prabhu, N.S.; Sharmila, K.; Kumaraswamy, S.; Somashekarappa, H.; Sayyed, M.; Al-Ghamdi, H.; Almuqrin, A.H.; Kamath, S.D. An examination of the radiation-induced defects and thermoluminescence characteristics of Sm<sub>2</sub>O<sub>3</sub> doped BaO–ZnO–LiF–B<sub>2</sub>O<sub>3</sub> glass system for  $\gamma$ -dosimetry application. *Opt. Mater.* **2021**, *118*, 111252. [[CrossRef](#)]
42. Singh, M.N.; Singh, L.R.; Barua, A.G. Effects of doping concentration on thermoluminescence parameters of CaAl<sub>2</sub>O<sub>4</sub>:Re<sup>3+</sup> (Re<sup>3+</sup> = Dy<sup>3+</sup>, Sm<sup>3+</sup>, Tm<sup>3+</sup>) prepared by combustion method. *Radiat. Phys. Chem.* **2021**, *188*, 109631. [[CrossRef](#)]
43. Środa, M.; Świontek, S.; Gieszczyk, W.; Bilski, P. The effect of CeO<sub>2</sub> on the thermal stability, structure and thermoluminescence and optically stimulated luminescence properties of barium borate glass. *J. Non-Crystalline Solids* **2019**, *517*, 61–69. [[CrossRef](#)]
44. Viesca-Villanueva, E.; Oliva, J.; Chavez, D.; Lopez-Badillo, C.; Gomez-Solis, C.; Mtz-Enriquez, A.; Garcia, C. Effect of Yb<sup>3+</sup> codopant on the upconversion and thermoluminescent emission of Sr<sub>2</sub>CeO<sub>4</sub>:Er<sup>3+</sup>, Yb<sup>3+</sup> phosphors. *J. Phys. Chem. Solids* **2020**, *145*, 109547. [[CrossRef](#)]
45. Dewangan, P.; Bisen, D.; Brahme, N.; Tamrakar, R.K.; Upadhyay, K.; Sharma, S.; Sahu, I.P. Studies on thermoluminescence properties of alkaline earth silicate phosphors. *J. Alloy Compd.* **2018**, *735*, 1383–1388. [[CrossRef](#)]
46. Ukare, R.S.; Dubey, V.; Zade, G.D.; Dhoble, S.J. PL Properties of Sr<sub>2</sub>CeO<sub>4</sub> with Eu<sup>3+</sup> and Dy<sup>3+</sup> for Solid State Lighting Prepared by Precipitation Method. *J. Fluoresc.* **2016**, *26*, 791–806. [[CrossRef](#)]
47. Nag, A.; Kutty, T.R.N. Photoluminescence of Sr<sub>2-x</sub>Ln<sub>x</sub>CeO<sub>4+x/2</sub> (Ln=Eu, Sm or Yb) prepared by a wet chemical method. *J. Mater. Chem.* **2003**, *13*, 370–376. [[CrossRef](#)]
48. Chen, R. Glow Curves with General Order Kinetics. *J. Electrochem. Soc.* **1969**, *116*, 1254–1257. [[CrossRef](#)]

**Disclaimer/Publisher’s Note:** The statements, opinions and data contained in all publications are solely those of the individual author(s) and contributor(s) and not of MDPI and/or the editor(s). MDPI and/or the editor(s) disclaim responsibility for any injury to people or property resulting from any ideas, methods, instructions or products referred to in the content.